Magnetophonon resonance on the phonon frequency difference in quasi-free-standing graphene

D. Żak,[1] W. Strupinski,[2] T. Ciuk,[3] R. Wojnarowska-Nowak,[1] P. Śliż,[1] G. Tomaka,[1] D. Ploch,[1] and E. M. Sheregii[1]

[1]*Centre for Microelectronic and Nanotechnology, University of Rzeszow, 1 Pigonia Str., 35-959 Rzeszow, Poland*

[2]*Physics Faculty, Warsaw University of Technology, Pl. Politechniki 1, 00-661 Warsaw, Poland*

[3]*Lukasiewicz Research Network - Institute of Electronic Materials Technology, Wolczynska 133, 01-919 Warsaw, Poland*

(Received 16 May 2019; revised 3 April 2020; accepted 4 January 2021; published 29 January 2021)

The structure of magnetoresistance curves as a function of magnetic field from 0 to 14 T at temperatures from 0.4 to 6.0 K for macroscopic samples of the quasi-free-standing (QFS) graphene monolayer on SiC substrate, are observed and analyzed, and also the spatial and depth frequency distribution of phonons have been measured using the micro-Raman spectroscopy (MRS). That one enables us to interpret the obtained resonance magnetoresistance curves based on the electron-phonon (e-p) interaction taking into account the actually observed phonon spectrum in researched samples: in the case of a linear e-p interaction the observation of the corresponding peaks on the $R_{xx}(B)$ curves is difficult because an uninterrupted background is created. While nonlinear MPR with simultaneous G-phonon emission and D-phonon absorption occur in magnetic fields below 5 T against the background of MPR due to linear e-p interaction as well as Shubnikov–de Haas oscillations.

DOI: 10.1103/PhysRevB.103.035432

I. INTRODUCTION

Properties of semiconductors and metals are significantly determined by the interaction of two crystal subsystems, electrons and phonons, affecting both optical and transport phenomena. Particularly, the scattering on the long wave longitudinal optical [LO(Γ)] phonons has an universal character in semiconductor crystals and two-dimensional systems [1,2] because the last one generates the macroscopic polarized pole and electrons interact very effectively with that and causes the resonance electron-phonon (e-p) interaction to manifest itself in such effects as magnetophonon resonance (MPR) in magnetoresistance [3–7] and in the magneto-optical case as pinnings or anticrossing effect of magneto-optical resonances (cyclotron resonance (CR) or interzone magnetoabsorption which sometimes are called the Johnson-Larsen effect [8]), as well as cyclotron phonon assisted resonance (CPR) [9]. All these effects are observed in the presence of strong magnetic field when the discrete Landau levels (LL) characterize the electron energy spectrum. MPR (in magnetoresistance) was widely used to research properties of bulk crystals [3–5] and two-dimensional systems [6,7]—either the electronic structure [3–7] or phonon spectrum as well as peculiarities of the e-p interaction [10–16].

In this context, the unique possibilities are presented by the graphene—on the one hand due to the extreme low effective mass of electrons (discrete electron energy spectrum takes place at comparatively low magnetic fields) and because of the complicated multimode nature of crystal lattice different from other two-dimensional systems, on the other hand [17–32]. This makes it possible to observe the above resonant effects (MPR in magnetoresistance and the Johnson-Larsen effect in magneto-optics) with the richness of phenomena unimaginable to those times: nine types of different electron transitions in the linear case (one-phonon processes) only [12]. It is not exhausted in the same rich means oscillatory structure of graphene because there are reports of other types of phonons, for example, flexural phonons which, as it turns out, can also interact with electrons [23]. On the other hand, a theoretical paper [24] dedicated to the phonon scattering of carriers in graphene was found that at high carrier densities elucidate the role of the different phonon modes in limiting electron mobility: the resistivity arising from scattering with transverse acoustic phonons is 2.5 times higher than that from longitudinal acoustic phonons (at nonresonant scattering caused by acoustic phonons with practically zero energies and momentum). How does this diversity of the phonon spectrum in graphene translate into MPR observation?

Correspondently different types of MPR (observed in the magnetoresistance as well as the Johnson-Larsen effect) have been recorded in graphene, for example, anticrossings effects when the Fermi level (FL) is crossed by the electron LL energy, equal to the phonon energy [18,25] as well as magneto-Raman scattering measurements on graphenelike locations on the surface of bulk graphite [26], and other results regarding this phenomenon in graphene: the B field dependence of the G line phonon renormalization of exfoliated single layer and bilayer graphene for low magnetic fields [27], tuning the e-p coupling in multilayer graphene with magnetic fields [28], phonon-mediated resonances at the magneto-Raman scattering [29], electron-phonon coupling in graphite via magnetophonon resonances [30], and measurement of filling-factor-dependent MPRs (also in the Raman spectroscopy) [31].

All these magneto-optical (including magneto-Raman) effects relate to the interaction of the current carriers with optical phonons in-plane in the graphene. Two-phonon processes were also observed in the case of Ref. [18]—MPR

(as the magneto-Raman scattering) on the sum of the phonon frequencies belonging to Γ or K point of the Brillouin zone (BZ) in graphene. However, another possibility—MPR on the frequency differences of the phonon modes [15,16] to these times—was not observed in the two-dimensional systems.

Some of the works (magneto-optical as CR [27,32] or based on magnetoresistance [33–36]) investigated quantum effects in graphene in the region of comparatively weak magnetic fields below 5 T. An observation of the magnetoresistance oscillations of exfoliated graphene, with a conduction channel width of 15 μm, has been interpreted by authors [33] as the resonant scattering of electrons on the TA phonons, which is unlikely in a linear case in semiconductors due to the lack of momentum conservation [1,2,18]. The recent publication [37], in which an attempt was made to theoretically justify such a resonance, did not dispel the existing doubts, but caused new ones. For example, how can one explain the experimental fact that the observed oscillations in [33] take place over a wide interval of temperatures (1.5–250 K). The MPR temperature observation interval is limited by the number of excited phonons in the crystal lattice on the one hand, which requires slightly higher temperatures according to the exponential factor $\exp -(h\omega_{\rm ph}/kT)$, where $h\omega_{\rm ph}$ is the energy of the phonons participating in the interaction, and the requirement to quantize the energy spectrum of electrons in a magnetic field on the other hand. In other words, a condition of a strong magnetic field in the quantum sense, $E_{n+1} - E_n \gg kT$, should take place which makes resonance testing impossible at higher temperatures. Since simultaneously the resonance condition is $E_{n+1} - E_n = nh\omega_{\rm ph}$ (where n is an integer 1, 2, 3, …), then it follows $nh\omega_{\rm ph} \gg kT$ which means that temperature cannot be high but sufficient for excitation of the crystal lattice. It automatically means a narrow temperature interval of MPR observation, the narrower the phonon energy the smaller is $h\omega_{\rm ph}$. In the case of longitudinal TA phonons that are few meV only, they shift the ability to observe MPR on the longitudinal TA phonons in the low temperature range—certainly below 77 K. This contradiction with experiment [33] suggests that the interpretation as MPR on TA phonons of the magnetoresistance oscillations observed on graphene in [33,37] at near room temperature is not appropriate.

Another group of publications [34–36] is dedicated to the problem of the carrier density fluctuations in graphene and, consequently, to the influence of these possible inhomogeneities on the longitudinal ρ_{xx} and transverse ρ_{xy} magnetoresistance with suspicion of oscillations (not periodic in this case [36]) in the same region of magnetic fields (under to 5 T). Therefore, it is interesting to explore $\rho_{xx}(B)$ and $\rho_{xy}(B)$ curves in the graphene in this range of magnetic fields with an aim to find realistic interpretations of observed magnetoresistance oscillations.

In this work we study the rich structure of the magnetoresistance curves as a function of magnetic field for quasi-free-standing (QFS) graphene monolayer on SiC [38] for which both the spatial and depth frequency distribution of the phonons in the same samples of QFS graphene have been obtained using the micro-Raman spectroscopy (MRS)—the method allows us to carefully examine the phonon subsystem as well as the homogeneity of the test layer. It is worth recalling that Raman scattering is done by exciting electrons by incident radiation, and then relaxing electrons (in the case of graphene, recombining electron-hole pairs) to excite the crystal lattice [39]. In this way, the MRS also checks the electron-phonon interaction in a single graphene layer which allowed us to interpret the obtained resonance magnetoresistance curves based on the e-p interaction taking into account the actually observed phonon spectrum in researched samples. The tested samples were definitely macroscopic ($1.5 \times 0.5\,{\rm mm}^2$) and the Hall measurement results did not depend on their size which was verified for a wide spectrum of the carrier density [40].

The paper is organized as follows. In Sec. II we briefly describe the growth technology of the QFS graphene, in Sec. III we present results of the MRS measurements of researched samples, Sec. IV is dedicated to the quantum Hall effect (QHE) and the Shubnikov–de Haas (SdH) oscillations, and Sec. V to the MPR and the analyses of the linear (Sec. V A) and two-phonon (Sec. V B) cases of the MPR in graphene.

II. SAMPLES

Graphene was epitaxially grown through the chemical vapor deposition (CVD) from hydrocarbons on the silicon face of a semi-insulating on-axis 6H-SiC substrate [38,40] (see also [41–43]). First an electrically inactive buffer layer was synthesized and only later *in situ* turned into a QFS monolayer through hydrogen atom intercalation [41] (see also [44–46]). The process of hydrogen atom intercalation activates the electrical properties of graphene. It reveals graphene's p-type conductivity and liberates its charge carriers [38,40]. The samples were electron-beam patterned to form equal-arm cross-shaped van der Pauw structures terminated with fivefold Cr/Au (20 nm/30 nm) ohmic contacts as the straight cross $1300 \times 500\,{\rm mm}^2$.

After MRS measurements all samples were passivated with a silicone encapsulate and mounted in custom-made packages. Figure 1 shows samples ready for magnetotransport measurements. Thus, the magnetotransport was measured for three series of samples in a wide temperature range from 0.25 to 200 K. Each series contained several samples and related to one growth process. For each measured sample, QHE and SdH oscillations in the range of magnetic fields up to 14 T were observed, it should be emphasized that the measurement devices were undoubtedly macroscopic and their sizes were selected optimally so that the results of the Hall effect measurements did not depend on the sample size.

In this way, two types of experiments—optical (MRS) and magnetoresistence (SdH)—allowed us to test several samples of three series of QFS graphene. During the magnetotransport measurements, a series of samples with high density of current carriers and, at the same time, relatively high mobility was selected. This made it possible to observe for this series the MPR with low transition energy in relatively higher magnetic fields (from 2.5 to 6 T) and unequivocally interpret them based on the known phonon energies (MRS) and precisely defined energies of electronic states in the magnetic field (SdH).

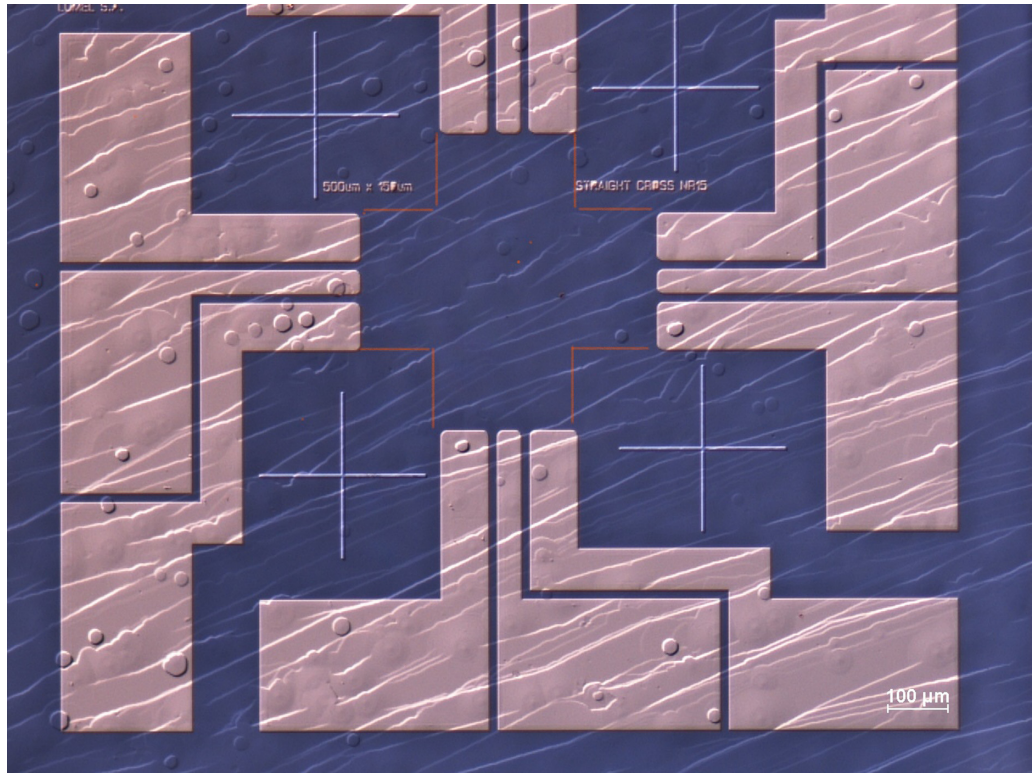

FIG. 1. Image of the measuring graphene sample obtained by scanning in an electron microscope. The red line marks the shape of the electrically active area.

III. PHONON SUBSYSTEM

The phonon subsystem has been verified by the MRS method mentioned above performed with the RENISHAW in a Via spectrometer equipped with a 488 nm laser source (0.06 W). The spot size was estimated at 3 μm. In this section the MRS data are shown in Figs. 2 and 3 for the series 3084 samples for which the magnetotransport measurement data will also be detailed in the next section. Figure 2(a) depicts Raman spectra obtained at six points on the surface of the sample. Two bands are clearly visible: G band at $1592 \pm 5\,\mathrm{cm}^{-1}$ and $2D$ band at $2723 \pm 7\,\mathrm{cm}^{-1}$, both are characteristic of graphene [19–22,47–51]. Figure 2(b) presents Raman maps of the above mentioned spectra. The band positions on the scale of wave numbers are the same with an accuracy of $15\,\mathrm{cm}^{-1}$ (less than 1% uncertainty) when the laser spot being moved by the 1 μm step cross through two sample areas with a total distance of 11 μm. Similar measurements were made for other areas of the tested sample, as well as for several other samples, and their repeatability confirms the high quality of the obtained graphene layers.

In the case of the depth frequency distribution, the MRS spectra [see Figs. 3(a) and 3(b)] were recorded at different focal lengths (focal point depth) of the laser beam under the surface of the sample (depth profile). Besides bands G and $2D$ (visible at the same frequencies as in Figs. 2(a) and 2(b), namely $\omega_G = 1592 \pm 5\,\mathrm{cm}^{-1}$ and $2\omega_D = 2723 \pm 7\,\mathrm{cm}^{-1}$, respectively), additionally the D line appears at $\omega_D = 1357 \pm 10\,\mathrm{cm}^{-1}$ for the focus depth of 1.5 μm—corresponding Raman spectrum is shown in Fig. 3(b). The appearance of the D line suggests the increasing influence of defects [20,47], whereas the fixed position of the G and $2D$ lines [see Fig. 3(a)] during the depth profiling is consistent with literature data [47–51].

IV. ELECTRON SUBSYSTEM

As was mentioned above, after the MRS measurements the samples were passivated with a silicone encapsulate to prevent uncontrolled environmental influence [43,52]. The magnetotransport measurements were performed in a cryomagnet system equipped with a superconducting coil and generating up to 14 T magnetic field (perpendicular to the graphene layer) [53]. The system maintains the sample's temperature in a range between 0.4 and 300 K. Direct current of 1 to 10 μA was applied to measure the longitudinal (R_{xx}) and Hall (R_{xy}) resistances. The data were averaged over the changing direction of the current with successive change of magnetic field.

The sign of the integer quantum Hall effect (IQHE) voltage observed clearly indicated hole transport which was caused by the intercalation of hydrogen into the structure of the graphene layers. In this section we present the magnetotransport data for two series of samples relating to two separate technological processes, respectively, named by us as 3084 and 3491. Typical curves of the IQHE and the Shubnikov–de Haas (SdH) oscillations for samples of series 3084 are shown in Fig. 4, sample 6H 3084. The $R_{xy}(B)$ curve of the Hall resistance clearly shows the plateau of IQHE with amazing stability in the temperature interval from 0.38 to 4.2 K. The maxima of the SdH oscillations are seen for each plateau, and in the low magnetic fields ($B < 4$ T) there is a substitute for an

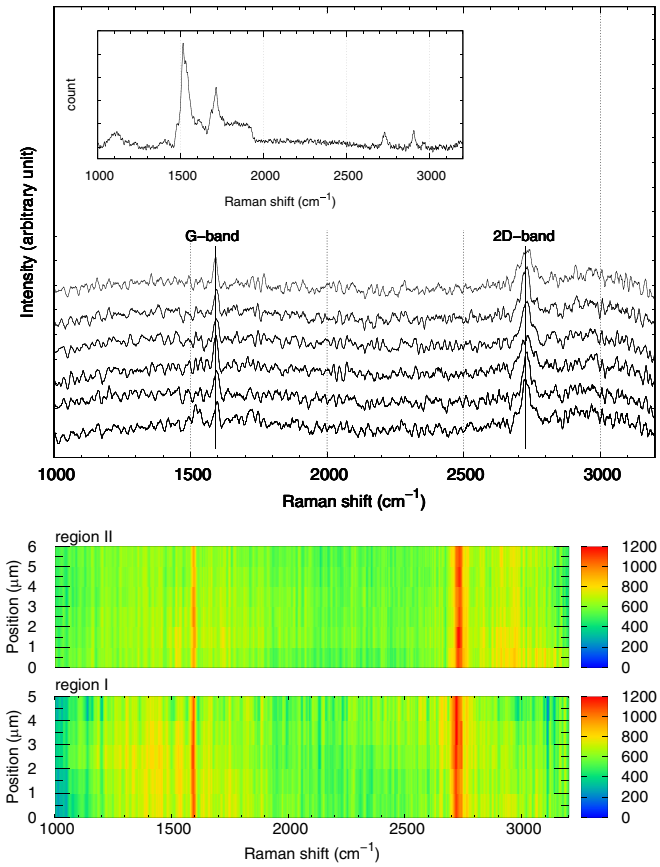

FIG. 2. (a) Raman spectra of QFS-monolayer graphene of series 3084 for six different points on the sample surface (inset: the spectrum without the SiC background subtraction). (b) Map of Raman spectra for the sample surface for two regions (I and II). The scan length in region I is 5 μm and in region II 6 μm, respectively. Distance between the measurement points is 1 μm.

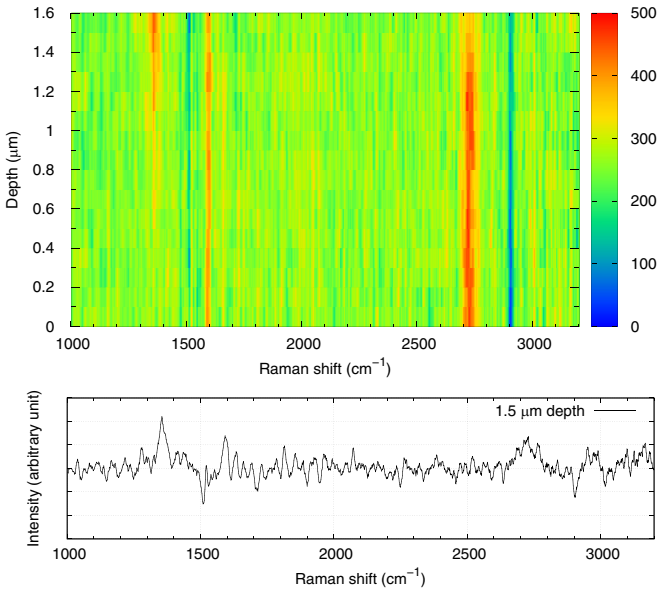

FIG. 3. (a) Dependence of the Raman spectrum from the focal point depth for QFS-monolayer graphene sample of series 3084, and (b) Raman spectrum of the QFS-monolayer graphene sample for the 1.5 μm focal point depth.

TABLE I. Parameters of the 2D hole gas in graphene (series 3084 and 3194).

Series of samples	Hole density (cm^{-2})	Hole mobility [$cm^2/(Vs)$]	Fermi level (meV)
3084	7.6×10^{12}	2918	332
3194	7.1×10^{12}	2026	298

additional (to SdH oscillations) series of peaks at 2.5, 1.2, and 0.8 T which are observed in Fig. 4 against the background of strong SdH oscillations.

In order to determine the fermion gas parameters for this series 3084, the curves for the sample 6H 3084 were selected, which are shown in Fig. 5(a). The charge carrier density and mobility are calculated from the slope of the Hall voltage at low magnetic fields and $R_{xx}(0)$ values at zero magnetic field. The values of hole density and mobility for both series of samples are presented in Table I: $7.6 \times 10^{12}\,cm^{-2}$ and $2918\,cm^2/(Vs)$ for 3084 series.

As it is shown in Fig. 5(a), the plateau of the IQHE and the Shubnikov–de Haas (SdH) oscillations are clearly visible up to high filling factors 62 for IQHE and 98 maxima for SdH. The position of the Fermi level (FL) and Landau levels (LLs) are shown in Fig. 5(b). The Landau levels energies $E_n(B)$, where B is the magnetic field, are calculated based on [54,55]

$$E_n(B) = \mathrm{sgn}(n)\sqrt{2e\hbar v_F^2|n|B}, \tag{1}$$

where $v_F = 1.0 \times 10^6$ m/s [50] is the Fermi velocity, n is the LL number with sign "+" for electrons and "−" for holes in graphene, and $\hbar$ is the reduced Planck constant.

It is evident that the depicted positions of FL accurately define the plateau in the IQHE curve and are observed according to a rule [54]:

$$R_{xy} = \mathrm{h}/\nu e^2, \;\; \nu = 4(n + 1/2), \tag{2}$$

where ν is the filling factor and e is the elementary charge.

The astonishingly high value of the IQHE filling factors (up to $\nu = 62$) observed in our QFS monolayer graphene indicate high quality layers. The relatively low Hall mobility could be attributed to high densities of holes: $7.6 \times 10^{12}\,cm^{-2}$ (corresponding to approximately $10^{19}\,cm^{-3}$ in bulk materials). Electron-electron interactions could decrease the Hall mobility at low magnetic fields as it was shown by authors [56,57].

Figure 6 depicts the magnetoresistance $R_{xx}(B)$ curve recorded for this layer in the range of low magnetic fields 0–6 T at temperature 0.4 K (without subtraction of the linear background but on an extended magnetoresistance scale). Two kinds of oscillations are clearly visible: SdH oscillations that extend to higher magnetic fields and magnetoresistance maxima (at 1.3, 2.5, and 4.0 T as was mentioned above) at lower magnetic fields. In Fig. 7 we present $R_{xx}(B)$ curves (also the original curves obtained without subtracting the linear background) in the range of low magnetic fields (0–6 T) for different temperatures from 0.35 to 4.2 K for this sample. It can be seen that these periodic in inverse magnetic field scale oscillations in the range of magnetic fields below 5 T are observed in a limited temperature interval—they disappear,

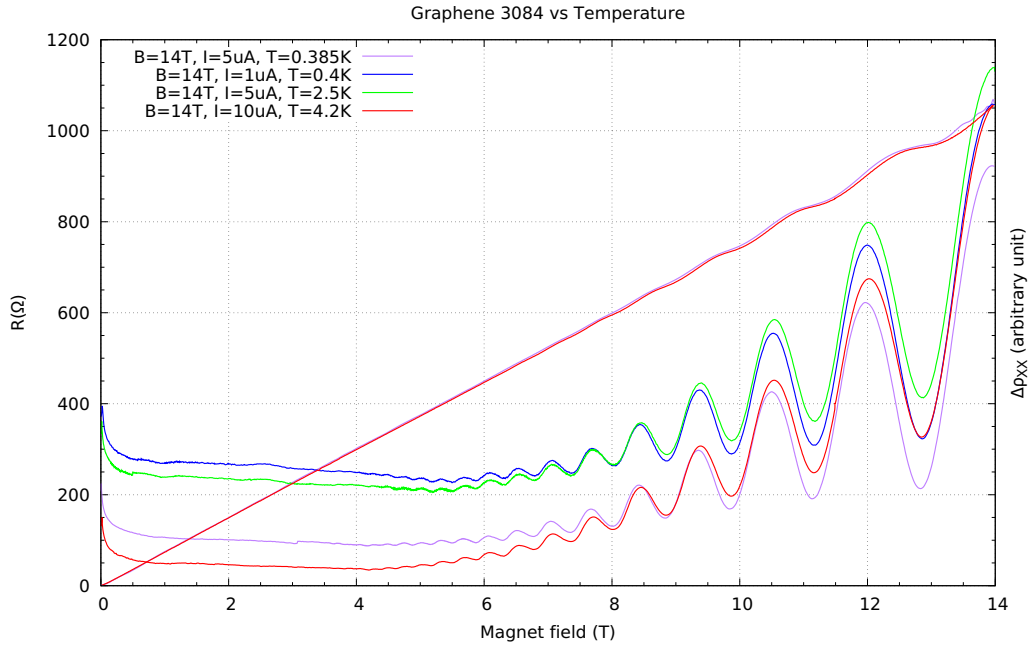

FIG. 4. Typical curves of the IQHE and the Shubnikov–de Haas (SdH) oscillations for samples of series 3084 (sample 6H) at temperatures from 0.4 to 10 K in the magnetic field 0–14 T.

practically, in fields above 3.5 K in contrast to those presented in [33] where the magnetoresistance oscillations are observed in a very wide temperature interval, namely from 5 to 250 K. A narrow temperature observation range of magnetoresistance oscillations is characteristic of MPR [3–7] as it was underlined in the Introduction.

For comparison, typical data for samples of series 3194 are presented in Fig. 8 for which the IQHE and SdH oscillations in the magnetotransport are observed also. These data allow us to determine the fermion gas parameters for the sample of series 3194: the carrier density $7.1 \times 10^{12}\,\mathrm{cm}^{-2}$, and the Hall mobility $2026\,\mathrm{cm}^2/(\mathrm{Vs})$ (see Table I). According to the much lower mobility of the fermions, no additional oscillations in the range of weak magnetic fields below 5 T (similar to those observed for the 3084 series, see Figs. 6 and 7) are visible in the curves in Fig. 8 for the samples from the 3194 series.

V. MAGNETOPHONON OSCILLATIONS

A. Linear e-p interaction

Theory: Theory of the electron-phonon (e-p) interaction in graphene in the linear case was developed by Basko [58] and Pound *et al.* [59,60] for the one-phonon Raman process as well as Ando [61] for the MPR in the magnetoresistance. In the last publication the electron states of the π bands near a $\boldsymbol{K}$ point in magnetic field B, perpendicular to the sheet, in the frame of the standard $\boldsymbol{kp}$ model, had been described and Eq. (1) for the electron states was used. The long-wavelength optical phonons have been considered on the basis of a valence force-field model and expression for self-energy was derived. Therefore, the interaction between optical phonons and an electron at the $\boldsymbol{K}$ point has been included in the form of the Hamiltonian used earlier [62] as well as the expressions (see [12] also) for the MPR conductivities σ_K^{xx}—including interaction with zone-edge phonons (D phonons), as well as σ_Γ^{xx}—including interaction with zone-center mode (G phonons), has been derived:

$$\sigma_K^{xx} = \frac{\sigma_K \gamma^2}{\hbar\omega_D l^2} \sum_{n=0}^{\infty}\sum_{m=0}^{\infty} K_{n,m}\delta_{\mathrm{K}}(E_n + E_m - \hbar\omega_D), \tag{3}$$

$$\sigma_\Gamma^{xx} = \frac{\sigma_\Gamma \gamma^2}{\hbar\omega_G l^2} \sum_{n=0}^{\infty}\sum_{m=0}^{\infty} K_{n,m}\delta_{\Gamma}(E_n + E_m - \hbar\omega_G), \tag{4}$$

where $\gamma = (\sqrt{3}/2)\gamma_0 a$; γ_0 is the transfer integral between π orbitals of the nearest-neighbor carbon atoms, a is the lattice constant, $K_{n,m} = \max(1,n) + \max(1,m)$, $N_K = n_B\hbar\omega_D$, $n_B = (e^{\beta\hbar\omega_D} - 1)^{-1}$, $\beta = 1/kT$,

$$\sigma_K = \lambda_K \frac{e^2}{\hbar} N_K(N_K+1)\frac{\hbar\omega_D}{kT}, \tag{5}$$

$$\sigma_\Gamma = \lambda_\Gamma \frac{e^2}{\hbar} N_\Gamma(N_\Gamma+1)\frac{\hbar\omega_G}{kT}, \tag{6}$$

where λ_K and λ_Γ are the dimensionless electron-phonon coupling parameters defined as

$$\lambda_K = \frac{36\sqrt{3}}{\pi}\frac{\hbar^2}{2Ma^2}\frac{1}{\hbar\omega_D}\left(\frac{\beta_K}{2}\right)^2, \tag{7}$$

$$\beta_K = -\frac{d\ln\gamma_0}{d\ln b}, \tag{8}$$

M is the mass of a carbon atom, and b is the bond length. The coupling parameter λ_Γ is given by Eq. (7) if the ω_D frequency is replaced with ω_G and the parameter β_K with β_Γ (β_Γ is practically the same as β_K in the nearest-neighbor tight-binding model [12]).

The total magnetoconductivity σ_{xx} is defined as the sum of the above two contribution from (3) and (4):

$$\sigma_{xx} = \sigma_K^{xx} + \sigma_\Gamma^{xx}. \tag{9}$$

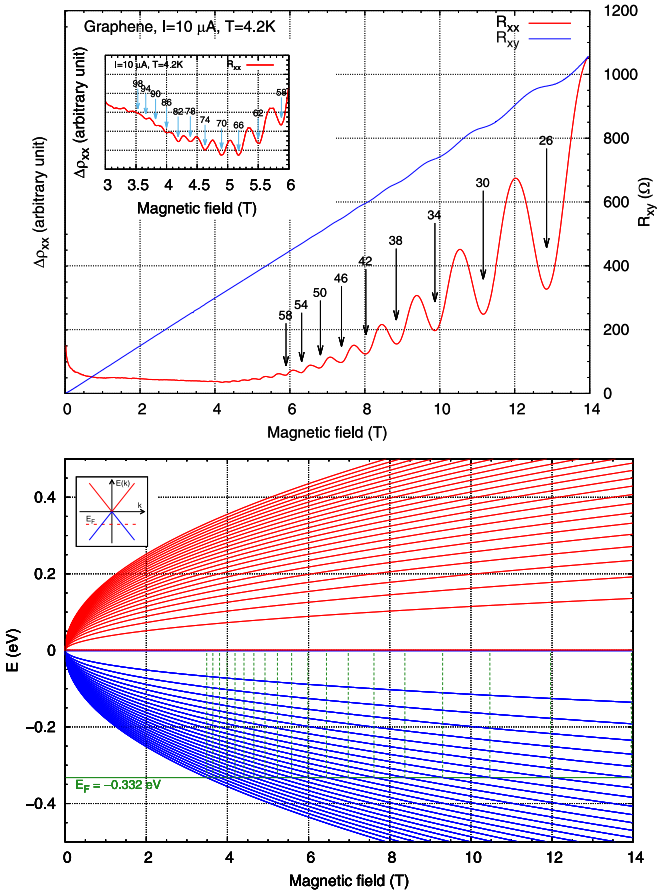

FIG. 5. (a) Experimental curves of the IQHE and SdH oscillations obtained: (a) for the QFS monolayer graphene sample 4H of the series 3084 at temperature 4.2 K [inset shows $R_{xx}(B)$ curve at temperature 4.2 K from 3 to 6 T magnetic field]. (b) The Landau levels energy $E_n(B)$ curves for electrons (red color) and holes (blue color) for the monolayer graphene calculated with parameter $v_F = 1.02 \times 10^6$ m/s. The IQHE interpretation with $E_F = -0.332$ eV (green line) is shown. Inset shows linear relation for energy E_k to wave vector k called Dirac cones with Fermi level for holes.

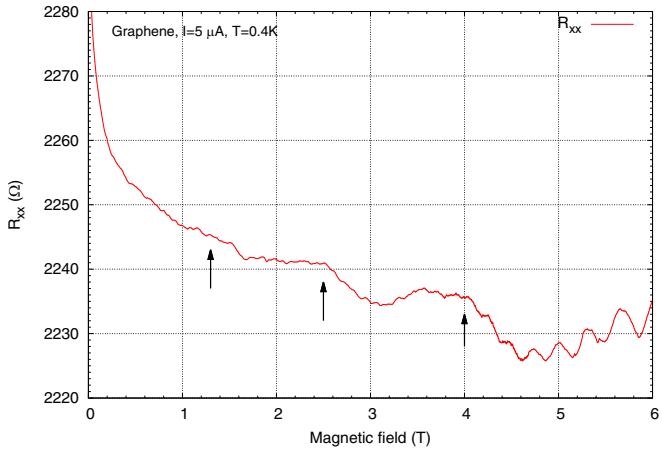

FIG. 6. Experimental curve of the $R_{xx}(B)$ magnetoresistance obtained at temperature 0.4 K for the QFS monolayer graphene sample 6H of series 3084 in the magnetic field region from 0 to 6 T and shown on an extended magnetoresistance scale in comparison with Fig. 4.

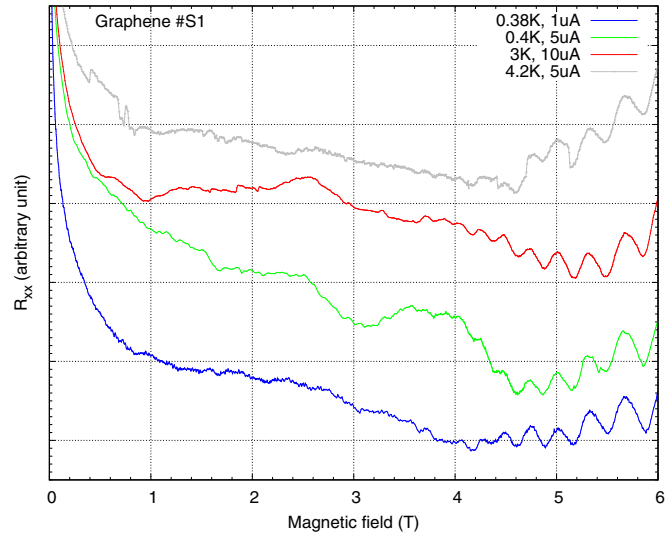

FIG. 7. Influence of temperature on the MPR oscillation amplitude in the range of weak magnetic fields up to 5 T for sample 6H series 3084.

It is well known [1–7] that magnetoresistivity ρ_{xx} in the case of strong magnetic field is proportional to magnetoconductivity σ_{xx}. So, $\rho_{xx} \sim \sigma_{xx}$, and the oscillatory part of the magnetoresistance as a function of magnetic field for the linear case can be written

$$\Delta\rho_{xx}^{\mathrm{lin}}(B) = \sum_{n=0}^{\infty}\sum_{m=0}^{\infty}\{A(\hbar\omega_D)K_{n,m}\delta_{\mathrm{K}}(E_n + E_m - \hbar\omega_D) + A(\hbar\omega_G)\, G_{n,m}\delta_{\mathrm{G}}(E_n + E_m - \hbar\omega_G)\}, \quad (10)$$

where the functions $A(\hbar\omega_D)$ and $A(\hbar\omega_G)$ replace the expressions before the sums in Eqs. (3) and (4), respectively.

Discussion: According to expression (10) and taking into account the general rule for the MPR in the degenerate electron gas, the electron transitions crossing the Fermi level only could occur in MPR, following [12], and these transitions could be called as

(1) principal ($-n \to 0$ and $0 \to +n$), where sign "−" refers to the valence band and "+" to the conduction band;

(2) symmetric ($-n \to +n$);

(3) asymmetric ($-n \to +m$, $-n \to -m$, *and* $+n \to +m$).

As follows from (10) two kinds of phonons could participate in these transitions:

LO phonons in the Γ point of the BZ (the *G* peak in MRS spectra) and the zone-edge optical phonons in the K point (the *D* peak).

The energies of these phonons are $\hbar\omega_G = 197$ meV and $\hbar\omega_D = 168$ meV, respectively, according to the Raman scattering data presented above. If we use these kind of phonons add a two *D* phonons combination (which is actively manifesting itself in the Raman spectra which means a high probability of participating in MPR). For the three types of magnetophonon transitions (principal, symmetric, and asymmetric) we obtain an uninterrupted palisade of transitions forming the continuous spectrum of magnetoresistance within the magnetic field range of 0 and 7 T as it is shown in Fig. 9: the

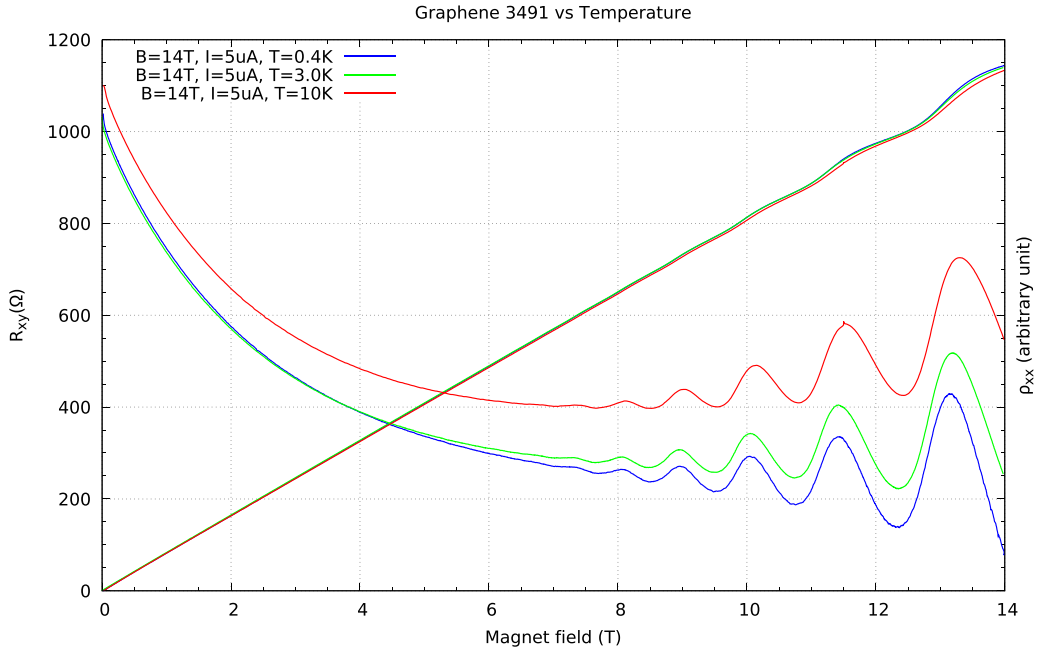

FIG. 8. Typical experimental curves of the $R_{xx}(B)$ magnetoresistance obtained at temperatures from 0.4 to 10 K in the magnetic field region from 0 to 6 T for the QFS monolayer graphene for the sample from series 3194.

first 80 Landau level (LL) curves calculated for electrons and holes in the monolayer graphene are presented, the horizontal line $E_F = -0.332\,\text{eV}$ shows the Fermi level position as in Fig. 5(b). Vertical lines indicate the electron transition positions in the scale of magnetic field between the LLs (the E_F intersection should be taken place) with the transition energies 168, 197, and 338 meV for the D, G, and $2D$ kinds of phonons, respectively. The black solid curve in Fig. 9 represents simulation of the $\Delta\rho_{xx}^{\text{lin}}(B)$ magnetoresistance according to Eq. (10) where the δ_K and δ_Γ functions are replaced by the Gaussian functions with properly selected temperature and collision bordering of the LLs for all the abovementioned

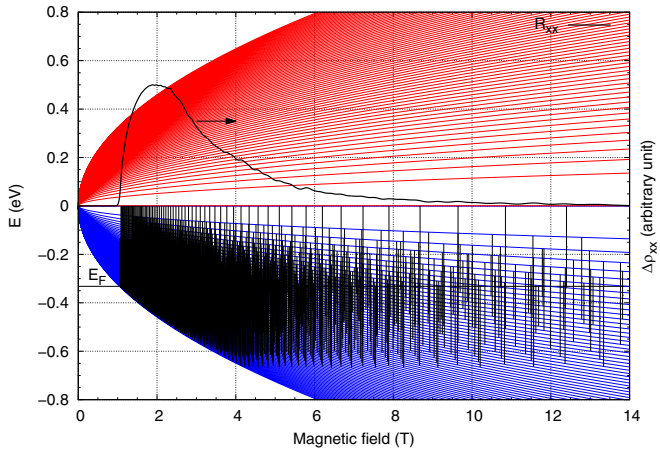

FIG. 9. The electron transition positions calculated for sample of series 3084 in the scale of magnetic field between the LLs (the E_F intersection takes place) with the transition energies 168, 197, and 338 meV for the D, G, and $2D$ kinds of phonons, respectively. The black solid curve represents simulation of the $R_{xx}(B)$ longitudinal magnetoresistance based on Eq. (10).

electron transitions. It can be seen that a dense palisade of electron transitions causes a continuous spectrum of magnetoresistance without the resonance peaks. This continuous magnetoresistance spectrum cannot explain the three clearly visible maxima in the region of magnetic fields from 0 to 6 T in the experimental $R_{xx}(B)$ curves presented in Figs. 6 and 7.

Participation of the TA phonons in the linear case: The inclusion of TA phonons (as well as LA phonons) in the resonant e-p interaction in the linear case as in Ref. [33] seems to be an artificial procedure with questionable physical justifications.

First, in previous MPR studies performed over 55 years in both volume crystals and two-dimensional systems, this effect was never seen on the TA phonons in the linear case [1–16].

Second, even if we suppose that the electrons in graphene will be selected in the linear dispersion of the TA phonons, only those that correspond to the electron momentum at the Fermi level ($k_F = q_F$, so called "Phonon-induced resistance oscillations in 2D systems …" [63]), in other words, only electrons with energy at the Fermi level participate in the e-p interaction for depicting resonances on the $R_{xx}(B)$ curves—the main hypothesis in the work [33,63]—the problem of the momentum conservation in the e-p interaction in the work [33] is reprimanded but not resolved satisfactorily as it is developed in [60] for acoustic phonons.

Third, in the previous results of the MPR researches in the degenerate two-dimensional semiconductor systems (see, for example, the works [5–7,10]) and according to the assumptions of Mori and Ando for the MPR in graphene [12], all transitions of electrons from the occupied states below the Fermi level take place, not just from the Fermi level itself, as it is assumed by authors [33], which means that the dispersion of the TA phonons will blur the resonance and it will not be visible but will create a continuous background.

Some similar doubts regarding the participation of acoustic phonons in the MPR in the Raman magnetoscattering are presented in the theoretical works [58–60,61]. As a consequence, the measurement result was dependent on the sample size and the fact that the oscillations are observed in a very wide temperature range (0.5–250 K) may indicate the possibility of a scattering mechanism other than in MPR. Such a wide temperature interval is characteristic for the phenomena caused by the breakdown of electronic orbits, e.g., due to a too narrow conduction channel: conductivity oscillations in a magnetic field are known as a magnetotransport analog of the Asbel-Kaner resonance [64].

B. High-order e-p interaction

In order to interpret the observed maxima in Figs. 6 and 7, we have to look for low energy electronic transitions. Such transitions could be realized by a higher-order process of the electron-phonon coupling considered by authors of several works dedicated to the multiphonon scattering in the Raman and magneto-Raman effect in graphite [65] and graphene [18,58,66,67].

Theory: Theory of multiphonon transitions for Raman scattering in graphene is presented by Basko [58]. The results of this theory are used for the multiple-phonon magneto-Raman scattering measurements [66] (although from the title of the article can be concluded that this is the MPR of magnetoresistance). Nevertheless, we can use the scheme of two-phonon transitions proposed by Basko [58] and Basko *et al.* [18] for graphene in the K and K' points of the BZ.

For example, an electron in the K point of BZ occupying one of the LL(n) below the FL absorbs the G phonon belonging to the Γ point (as noted in the Introduction, long-wave LO phonons, i.e., phonons in the center of BZ form a macroscopic polarizing field with which electrons interact effectively), after that it emits the D phonon of lower energy and maximal momentum (belong to the K point) and transfers to the opposite K' point of BZ to keep up the momentum, where it occupies a LL(m) above the FL (see Fig. 10). The energy conservation equation for the initial and final states of the process is given by

$$E_m - E_n = \hbar\omega_{\rm ph}(G) - \hbar\omega_{\rm ph}(D) \tag{11}$$

The difference between the G-phonon energy $\hbar\omega_{\rm ph}(G)$–197 meV and D-phonon energy $\hbar\omega_{\rm ph}(D)$–168 meV, according our measurements, is

$$\hbar\Delta\omega(G-D) = 29\ \text{meV}. \tag{12}$$

It is obvious that the electron transitions (with such a small energy in our case of the graphene with the hole conductivity) are only possible inside the valence band near FL: asymmetric transitions $-n \rightarrow -m$. For this the oscillating part of magnetoresistance responsible for these transitions can be written

$$\Delta\rho_{xx}^{\rm nonlin} = \sum_{n=-\infty}^{0}\sum_{m=-\infty}^{0}\{A'[\hbar\Delta\omega(G-D)]K_{n,m} \times \delta_{K\Gamma}[E_n + E_m - \hbar\Delta\omega(G-D)]\}, \tag{13}$$

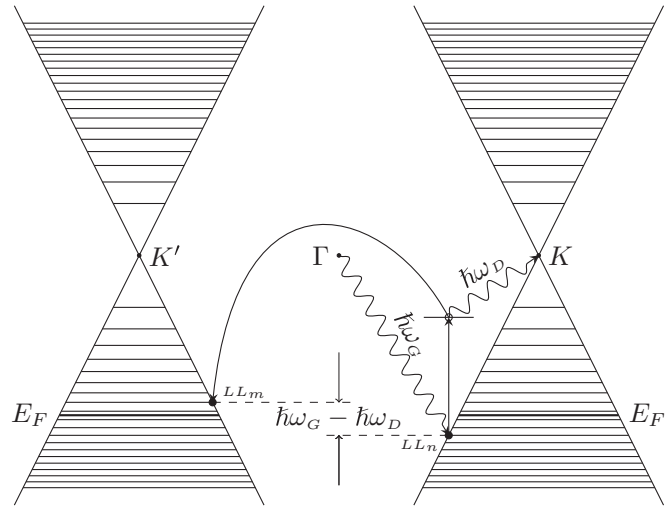

FIG. 10. Scheme of the electron transition with high-order e-p interaction between two Landau levels (of the Landau number n and m : LL_n and LL_m, respectively) in p-type monolayer graphene, series 3084. Electron occupying the LL_n in the K point absorbs phonon from the Γ point with energy $\bar{\text{h}}\omega(G)$ and occupies the virtual level passing the E_F without change of the momentum; after that it emits the D phonon belonging to the K point with energy $\bar{\text{h}}\omega(D)$ and relaxes down to the LL_m in the K' point with momentum law conservation. Energy difference between LL_n and LL_m is equal to $\bar{\text{h}}\omega(G) - \bar{\text{h}}\omega(D)$ which means the energy conservation.

with the dimensionless electron-phonon coupling parameters

$$\lambda_{K\Gamma} = \left[\frac{36\sqrt{3}}{\pi}\frac{\hbar^2}{2Ma^2}\frac{1}{\hbar\Delta\omega(G-D)}\left(\frac{\beta_{K\Gamma}}{2}\right)^2\right]^2, \tag{14}$$

where $N_{K\Gamma} = n_B\,\hbar\Delta\omega(G-D)$, $\beta_{K\Gamma} = \beta_K = \beta_\Gamma$ as it was defined above in Sec. V A.

Experiment and discussion: Possible electron transitions between the LLs in nonlinear processes according to (13) with the phonon frequency difference (12) in graphene are shown in Fig. 11. A corresponding simulation curve of the $\Delta\rho_{xx}^{\rm nonlin}(B)$ oscillating part of the magnetoresistance, which takes into account the temperature and collision broadening of the LLs, as it was done for the linear case above, is shown in Fig. 11 also. As can be seen in Fig. 11, the theoretical curve perfectly reflects the experimental curve in general: three characteristic double peaks at about 1.5, 2.5, and 4 T. The next peak should be at 7 T but it is masked by the Shubnikov–de Haas oscillations. Theoretical double peaks are slightly shifted towards stronger magnetic fields compared to experimental ones but this shift is within the half-width of the peaks observed.

In this way, the assumption was that the MPR takes place with a simultaneous absorption and emission of two phonons belonging to two equivalent points of the BZ of graphene. These processes occur on a continuous background of the electron transitions, described above in Sec. V A, between the LLs with emission (absorption) of one phonon (see Fig. 10). It may seem that the probability of a process with the G-phonon absorption at such a low temperature (0.4 K) is low but one should take into account that in the graphene lattice the

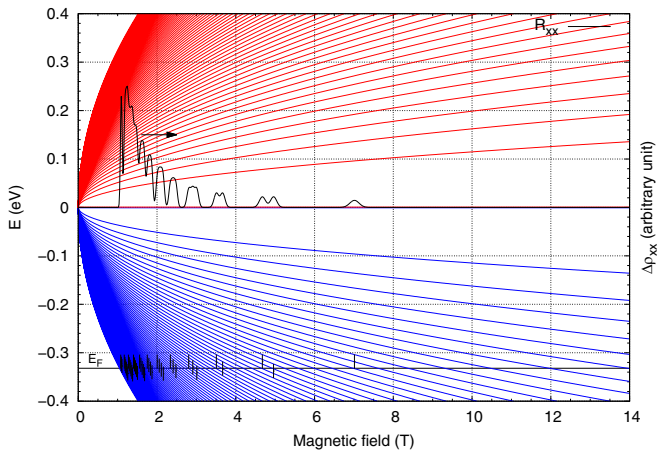

FIG. 11. The high-order electron transitions positions in the magnetic fields calculated for QFS graphene, series 3084. The LL energy curves and the $E_F = -0.332$ eV are as in Fig. 5(b). Vertical lines indicate positions in the magnetic field scale of the high-order electron transitions between LLs with the transition energy 29 meV which is the energy difference between the G and D kinds of phonons (phonon energies: 197 and 168 meV, respectively). The black solid curve represents the simulation of the longitudinal magnetoresistance $R_{xx}(B)$ as a sum of the Gaussians for these transitions taking into account the temperature and collision broadening of the LLs.

process of phonon emission takes place constantly as a result of the electron relaxation from higher to lower LLs [68,69]. This means the graphene lattice is constantly excited which makes the phonon absorption process possible even at low temperatures.

The value of $\hbar\Delta\omega(G-D)$ in (14) is small (29 meV which, however, is twice as much as in the case of TA phonons) which causes a quick lowering with the temperature increase in the MPR on the phonon frequency difference amplitude, which is observed in Fig. 7. Resonance is possible to observe in a narrow temperature range, from 0.4 to 3.0 K, because it is limited, as was mentioned above, by the number of phonons on the low temperature side and the temperature broadening of Landau levels on the higher temperature side. The last one is especially important at small magnetic fields as well as a sufficiently high mobility of the current carriers.

Therefore, graphene is characterized at low temperatures (0.3–4.2 K) and at low magnetic fields (up to 5 T) by specific MPR with a simultaneous absorption and emission of two kinds of phonons—emission of G and absorption of D phonons.

VI. CONCLUSION

Various types of MPR take place in the graphene in the case of a linear e-p interaction at low temperatures (0.4–4.2 K), constantly causing excitation of the crystal lattice and preventing the observation of the corresponding separated peaks caused by the one-phonon MPR on the $R_{xx}(B)$ curves in the magnetic field $B < 5$ T because an uninterrupted background is created. The Shubnikov–de Haas oscillations can be observed against this background in the discussed range of the magnetic field (but more so in the higher fields) at temperatures below 2 K. However, MPRs with G-phonon emission and simultaneous D-phonon absorption occur in the magnetic fields below 5 T as has been shown in this work. These high-order MPR oscillations were researched on graphene samples with a comparably high hole density and mobility, the size of which corresponded to the criteria of magnetotransport measurements and are consistent with the theory of multiphonon resonance developed in Refs. [18,58].

ACKNOWLEDGMENT

The research leading to these results has received funding from the National Centre for Research and Development under Grant Agreement No. LIDER 0168/L-8/2016 for project "Graphene on silicon carbide devices for magnetic field detection in extreme temperature conditions."

[1] B. Gantmacher and Y. Levinson, *Carrier Scattering in Metals and Semiconductors* (North-Holland, New York, 1987).
[2] Y. B. Levinson and E. I. Rashba, Electron-phonon and exciton-phonon bound states, Rep. Progr. Phys. **36**, 1499 (1973).
[3] Yu. A. Firsov, V. L. Gurevich, R. V. Parfeniev, and S. S. Shalyt, Investigation of a New Type of Oscillations in the Magnetoresistanc, Phys. Rev. Lett. **12**, 660 (1964).
[4] R. A. Wood and R. A. Stradling, The magnetophonon effect in III-V semiconducting compounds, J. Phys. C Solid State Phys. **1**, 1711 (1968).
[5] Y. A. Firsov, V. L. Gurevich, R. V. Parfeniev, and I. M. Tsidlikovskii, in *Landau Level Spectroscopy*, edited by V. M. Agranovich and A. A. Maradudin, Vol. 27.2 in Series: Modem, Problems in Condensed Matter Sciences (North-Holland, Amsterdam, 1991), pp. 1181–1302.
[6] R. J. Nicholas, see Ref. [5], pp. 777–816.
[7] D. C. Tsui, T. Englert, A. Y. Cho, and A. C. Gossard, Observation of Magnetophonon Resonances in a Two-Dimensional Electronic System, Phys. Rev. Lett. **44**, 341 (1980).
[8] E. J. Johnson and D. M. Larsen, Polaron Induced Anomalies in the Interband Magnetoabsorption of InSb, Phys. Rev. Lett. **16**, 655 (1966).
[9] F. G. Bass and I. B. Levinson, Cyclotron-phonon resonance in semiconductors, Sov. Phys. JETP **22**, 636 (1966).
[10] D. Ploch, E. M. Sheregii, M. Marchewka, M. Woźny, and G. Tomaka, Magnetophonon resonances in double quantum wells, Phys. Rev. B **79**, 195434 (2009).
[11] Yu. O. Ugrin and E. M. Sheregii, Magnetophonon resonance on three types of carriers in p-InSb, Phys. Status Solidi (b) **166**, 2491991.
[12] N. Mori and T. Ando, Magnetophonon resonance in monolayer graphene, J. Phys. Soc. Jpn. **80**, 044706 (2011).
[13] E. M. Sheregii and Yu. O. Ugrin, CdHgTe phonon-spectra research by means of magnetophonon resonance, Solid State Commun. **83**, 1043 (1992).

[14] M. A. Zudov, I. V. Ponomarev, A. L. Efros, R. R. Du, J. A. Simmons, and J. L. Reno, New Class of Magnetoresistance Oscillations: Interaction of a Two-Dimensional Electron Gas with Leaky Interface Phonons, Phys. Rev. Lett. **86**, 3614 (2001).

[15] E. M. Sheregii, Yu. O. Ugrin, D. D. Shuptar, and O. M. Leshko, Magnetophonon resonace in mixed optical modes of cadmium and mercury tellurides in $Cd_xHg_{1-x}Te$, JETP Lett. **47**, 711 (1988).

[16] E. M. Sheregii, Role of non-linear electron-phonon interaction in semiconductors, Europhys. Lett. **18**, 325 (1992).

[17] M. I. Katsnelson, *Graphene* (Cambridge University Press, Cambridge, 2012).

[18] D. M. Basko, P. Leszczynski, C. Faugeras, J. Binder, A. A. L. Nicolet, P. Kossacki, M. Orlita, and M. Potemski, Multiple magneto-phonon resonances in graphene, 2D Mater. **3**, 015004 (2016).

[19] A. C. Ferrari, J. C. Meyer, V. Scardaci, C. Casiraghi, M. Lazzeri, F. Mauri, S. Piscanec, D. Jiang, K. S. Novoselov, S. Roth, and A. K. Geim, Raman Spectrum of Graphene and Graphene Layers, Phys. Rev. Lett. **97**, 187401 (2006).

[20] Z. H. Ni, W. Chen, X. F. Fan, J. L. Kuo, T. Yu, A. T. S. Wee, and Z. X. Shen, Raman spectroscopy of epitaxial graphene on a SiC substrate, Phys. Rev. B **77**, 115416 (2008).

[21] J. Röhrl, M. Hundhausen, K. V. Emtsev, T. Seyller, R. Graupner, and L. Ley, Raman spectra of epitaxial graphene on SiC(0001), Appl. Phys. Lett. **92**, 201918 (2008).

[22] L. Malard, M. Pimenta, G. Dresselhaus, and M. Dresselhaus, Raman spectroscopy in graphene, Phys. Rep. **473**, 51 (2009).

[23] E. Mariani and F. von Oppen, Flexural Phonons in Free-Standing Graphene, Phys. Rev. Lett. **100**, 076801 (2008).

[24] C.-H. Park, N. Bonini, T. Sohier, G. Samsonidze, B. Kozinsky, M. Calandra, F. Mauri, and N. Marzari, Electron–phonon interactions and the intrinsic electrical resistivity of graphene, Nano Lett. **14**, 1113 (2014).

[25] M. O. Goerbig, J.-N. Fuchs, K. Kechedzhi, and V. I. Fal'ko, Filling-Factor-Dependent Magnetophonon Resonance in Graphene, Phys. Rev. Lett. **99**, 087402 (2007).

[26] J. Yan, S. Goler, T. D. Rhone, M. Han, R. He, P. Kim, V. Pellegrini, and A. Pinczuk, Observation of Magnetophonon Resonance of Dirac Fermions in Graphite, Phys. Rev. Lett. **105**, 227401 (2010).

[27] C. Neumann, R. M. Drögeler, B. Terrés, K. Watanabe, T. Taniguchi, B. Beschoten, S. V. Rotkin, and C. Stampfer, Low B field magnetophonon resonances in single-layer and bilayer graphene, Nano Lett. **15**, 1547 (2015).

[28] C. Faugeras, M. Amado, P. Kossacki, M. Orlita, M. Sprinkle, C. Berger, W. A. de Heer, and M. Potemski, Tuning the Electron-Phonon Coupling in Multilayer Graphene with Magnetic Fields, Phys. Rev. Lett. **103**, 186803 (2009).

[29] C. Faugeras, M. Amado, P. Kossacki, M. Orlita, M. Kuhne, A. A. L. Nicolet, Yu. I. Latyshev, and M. Potemski, Magneto-Raman Scattering of Graphene on Graphite: Electronic and Phonon Excitations, Phys. Rev. Lett. **107**, 036807 (2011).

[30] Y. Kim, Y. Ma, A. Imambekov, N. G. Kalugin, A. Lombardo, A. C. Ferrari, J. Kono, and D. Smirnov, Magnetophonon resonance in graphite: High-field Raman measurements and electron-phonon coupling contributions, Phys. Rev. B **85**, 121403(R) (2012).

[31] Y. Kim, J. M. Poumirol, A. Lombardo, N. G. Kalugin, T. Georgiou, Y. J. Kim, K. S. Novoselov, A. C. Ferrari, J. Kono, O. Kashuba, V. I. Fal'ko, and D. Smirnov, Measurement of Filling-Factor-Dependent Magnetophonon Resonances in Graphene Using Raman Spectroscopy, Phys. Rev. Lett. **110**, 227402 (2013).

[32] M. Witowski, M. Orlita, R. Stępniewski, A. Wysmołek, J. M. Baranowski, W. Strupiński, C. Faugeras, G. Martinez, and M. Potemski, Quasiclassical cyclotron resonance of Dirac fermions in highly doped graphene, Phys. Rev. B **82**, 165305 (2010).

[33] P. Kumaravadivel, M. T. Greenaway, D. Perello, A. Berdyugin, J. Birkbeck, J. Wengraf, S. Liu, J. H. Edgar, A. K. Geim, L. Eaves, and R. K. Kumar, Strong magnetophonon oscillations in extra-large graphene, Nat. Commun. **10**, 3334 (2019).

[34] Y.-B. Zhou, H.-C. Wu, D.-P. Yu, and Z.-M. Liao, Magnetoresistance in graphene under quantum limit regime, Appl. Phys. Lett. **102**, 093116 (2013).

[35] Z. Tan, C. Tan, L. Ma, G. T. Liu, L. Lu, and C. L. Yang, Shubnikov–de Haas oscillations of a single layer graphene under dc current bias, Phys. Rev. B **84**, 115429 (2011).

[36] A. Nachawaty, M. Yang, W. Desrat, S. Nanot, B. Jabakhanji, D. Kazazis, R. Yakimova, A. Cresti, W. Escoffier, and B. Jouault, Magnetic field driven ambipolar quantum Hall effect in epitaxial graphene close to the charge neutrality point, Phys. Rev. B **96**, 075442 (2017).

[37] M. T. Greenaway, R. K. Kumar, P. Kumaravadivel, A. K. Geim, and L. Eaves, Magnetophonon spectroscopy of Dirac fermion scattering by transverse and longitudinal acoustic phonons in graphene, Phys. Rev. B **100**, 155120 (2019).

[38] W. Strupinski, K. Grodecki, A. Wysmolek, R. Stepniewski, T. Szkopek, P. E. Gaskell, A. Grüneis, D. Haberer, R. Bozek, J. Krupka, and J. M. Baranowski, Graphene epitaxy by chemical vapor deposition on SiC, Nano Lett. **11**, 1786 (2011).

[39] J. L. Birman, *Theory of Crystal Space Groups and Infra-red and Raman Lattice Processes of Insulating Crystals* (Springer, Berlin, 1974).

[40] T. Ciuk and W. Strupinski, Statistics of epitaxial graphene for Hall effect sensors, Carbon **93**, 1042 (2015).

[41] C. Riedl, C. Coletti, T. Iwasaki, A. A. Zakharov, and U. Starke, Quasi-Free-Standing Epitaxial Graphene on SiC Obtained by Hydrogen Intercalation, Phys. Rev. Lett. **103**, 246804 (2009).

[42] T. Ciuk, O. Petruk, A. Kowalik, I. Jozwik, A. Rychter, J. Szmidt, and W. Strupinski, Low-noise epitaxial graphene on SiC Hall effect element for commercial applications, Appl. Phys. Lett. **108**, 223504 (2016).

[43] T. Ciuk, P. Caban, and W. Strupinski, Charge carrier concentration and offset voltage in quasi-free-standing monolayer chemical vapor deposition graphene on SiC, Carbon **101**, 431 (2016).

[44] S. Watcharinyanon, C. J. Virojanadara, A. Osiecki, A. Zakharov, R. Yakimova, R. Uhrberg, and L. Johansson, Hydrogen intercalation of graphene grown on 6H-SiC(0001), Surf. Sci. **605**, 1662 (2011).

[45] N. Ray, S. Shallcross, S. Hensel, and O. Pankratov, Buffer layer limited conductivity in epitaxial graphene on the Si face of SiC, Phys. Rev. B **86**, 125426 (2012).

[46] F. Speck, J. Jobst, F. Fromm, M. Ostler, D. Waldmann, M. Hundhausen, H. B. Weber, and T. Seyller, The quasi-free-standing nature of graphene on H-saturated SiC (0001), Appl. Phys. Lett. **99**, 122106 (2011).

[47] L. G. Cançado, A. Jorio, E. H. M. Ferreira, F. Stavale, C. A. Achete, R. B. Capaz, M. V. O. Moutinho, A. Lombardo, T. S. Kulmala, and A. C. Ferrari, Quantifying defects in graphene via Raman spectroscopy at different excitation energies, Nano Lett. **11**, 3190 (2011).

[48] K. Grodecki, Raman spectroscopy of graphene, Electron. Mater. (pol.) **41**, 47 (2013).

[49] S. Goler, C. Coletti, V. Piazza, P. Pingue, F. Colangelo, V. Pellegrini, K. V. Emtsev, S. Forti, U. Starke, F. Beltram, and S. Heun, Revealing the atomic structure of the buffer layer between SiC(0001) and epitaxial graphene, Carbon **51**, 249 (2013).

[50] F. Fromm, P. Wehrfritz, M. Hundhausen, and T. Seyller, Looking behind the scenes: Raman spectroscopy of top-gated epitaxial graphene through the substrate, New J. Phys. **15**, 113006 (2013).

[51] J. Kunc, M. Rejhon, and P. Hlídek, Hydrogen intercalation of epitaxial graphene and buffer layer probed by mid-infrared absorption and Raman spectroscopy, AIP Adv. **8**, 045015 (2018).

[52] T. Ciuk, A. Kozlowski, P. P. Michalowski, W. Kaszub, M. Kozubal, Z. Rekuc, J. Podgorski, B. Stanczyk, K. Przyborowska, I. Jozwik, A. Kowalik, and P. Kaminski, Thermally activated double-carrier transport in epitaxial graphene on vanadium-compensated 6h-SiC as revealed by Hall effect measurements, Carbon **139**, 776 (2018).

[53] G. Tomaka, J. Grendysa, P. Śliż, C. R. Becker, J. Polit, R. Wojnarowska, A. Stadler, and E. M. Sheregii,High temperature stability of the semiconductors with strong spin-orbital interaction, Phys. Rev. B **93**, 205419 (2016).

[54] Y. Zhang, Y.-W. Tan, H. L. Stormer, and P. Kim, Experimental observation of the quantum Hall effect and Berry's phase in graphene, Nature (London) **438**, 201 (2005).

[55] A. H. C. Neto, F. Guinea, N. M. R. Peres, K. S. Novoselov, and A. K. Geim, The electronic properties of graphene, Rev. Mod. Phys. **81**, 109 (2009).

[56] J. L. Tedesco, B. L. VanMil, R. L. Myers-Ward, J. M. McCrate, S. A. Kitt, P. M. Campbell, G. G. Jernigan, J. C. Culbertson, C. R. Eddy, and D. K. Gaskill, Hall effect mobility of epitaxial graphene grown on silicon carbide, Appl. Phys. Lett. **95**, 122102 (2009).

[57] C. Yu, J. Li, K. Gao, T. Lin, Q. Liu, S. Dun, Z. He, S. Cai, and Z. Feng, Observation of quantum Hall effect and weak localization in p-type bilayer epitaxial graphene on SiC(0001), Solid State Commun. **175–176**, 119 (2013).

[58] D. M. Basko, Theory of resonant multiphonon Raman scattering in graphene, Phys. Rev. B **79**, 205428 (2009).

[59] A. Pound, J. P. Carbotte, and E. J. Nicol, Effects of electron-phonon coupling on Landau levels in graphene, Phys. Rev. B **84**, 085125 (2011).

[60] A. Pound, J. P. Carbotte, and E. J. Nicol, Magneto-optical conductivity in graphene including electron-phonon coupling, Phys. Rev. B **85**, 125422 (2012).

[61] T. Ando, Magnetic Oscillation of Optical Phonon in Graphene, J. Phys. Soc. Jpn. **76**, 024712 (2007).

[62] K. Ishikawa and T. Ando, Optical Phonon Interacting with Electrons in Carbon Nanotubes, J. Phys. Soc. Jpn. **75**, 084713 (2006).

[63] A. T. Hatke, M. A. Zudov, L. N. Pfeiffer, and K. W. West, Phonon-Induced Resistance Oscillations in 2D Systems with a Very High Electron Mobility, Phys. Rev. Lett. **102**, 086808 (2009).

[64] I. V. Andreeva, V. M. Murav'eva, I. V. Kukushkina, J. H. Smet, K. von Klitzing, and V. Umanskii, Contactless measurement of the conductivity of two-dimensional electrons in the regime of microwave-induced giant magnetoresistance oscillations, JETP Lett. **88**, 616 (2008).

[65] C. Thomsen and S. Reich, Double Resonant Raman Scattering in Graphite, Phys. Rev. Lett. **85**, 5214 (2000).

[66] C. Faugeras, P. Kossacki, D. M. Basko, M. Amado, M. Sprinkle, C. Berger, W. A. de Heer, and M. Potemski, Effect of a magnetic field on the two-phonon Raman scattering in graphene, Phys. Rev. B **81**, 155436 (2010).

[67] A. Das, B. Chakraborty, and A. K. Sood, Raman spectroscopy of graphene on different substrates and influence of defects, Phys. Rev. B **79**, 155417 (2009).

[68] M. Breusing, S. Kuehn, T. Winzer, E. Malić, F. Milde, N. Severin, J. P. Rabe, C. Ropers, A. Knorr, and T. Elsaesser, Ultrafast nonequilibrium carrier dynamics in a single graphene layer, Phys. Rev. B **83**, 153410 (2011).

[69] P. Borowik, J.-L. Thobel, and L. Adamowicz, Monte Carlo study of electron relaxation in graphene with spin polarized, degenerate electron gas in presence of electron-electron scattering, Semicond. Sci. Technol. **32**, 125006 (2017).